AGU PUBLICATIONS

Geophysical Research Letters

RESEARCH LETTER

10.1002/2014GL060196

Key Points:
- The north-south asymmetry of Mercury's magnetic field is explained
- Coexistence of two columnar convection modes gives rise to this asymmetry
- Volumetric buoyancy and CMB heat flow heterogeneity are the key ingredients

Supporting Information:
- Readme
- Figure S1
- Figure S2
- Text S1

Correspondence to:
H. Cao,
haocao@ucla.edu

Citation:
Cao, H., J. M. Aurnou, J. Wicht, W. Dietrich, K. M. Soderlund, and C. T. Russell (2014), A dynamo explanation for Mercury's anomalous magnetic field, *Geophys. Res. Lett.*, *41*, doi:10.1002/2014GL060196.

Received 10 APR 2014
Accepted 21 MAY 2014
Accepted article online 2 JUN 2014

A dynamo explanation for Mercury's anomalous magnetic field

Hao Cao[1,2], Jonathan M. Aurnou[1], Johannes Wicht[3], Wieland Dietrich[4], Krista M. Soderlund[5], and Christopher T. Russell[1,2]

[1]Department of Earth, Planetary, and Space Sciences, University of California, Los Angeles, California, USA, [2]Institute of Geophysics and Planetary Physics, University of California, Los Angeles, California, USA, [3]Justus-von-Liebig-Weg 3, Max Planck Institute for Solar System Research, Göttingen, Germany, [4]Department of Applied Mathematics, University of Leeds, Leeds, UK, [5]Institute for Geophysics, John A. and Katherine G. Jackson School of Geosciences, University of Texas at Austin, Austin, Texas, USA

Abstract Recent MErcury Surface, Space ENvironment, GEochemistry, and Ranging (MESSENGER) measurements have shown that Mercury's magnetic field is axial-dominant, yet strongly asymmetric with respect to the equator: the field strength in the Northern Hemisphere is approximately 3 times stronger than that in the Southern Hemisphere. Here we show that convective dynamo models driven by volumetric buoyancy with north-south symmetric thermal boundaries are capable of generating quasi-steady north-south asymmetric magnetic fields similar to Mercury's. This symmetry breaking is promoted and stabilized when the core-mantle boundary heat flux is higher at the equator than at high latitudes. The equatorially asymmetric magnetic field generation in our dynamo models corresponds to equatorially asymmetric kinetic helicity, which results from mutual excitation of two different modes of columnar convection. Our dynamo model can be tested by future assessment of Mercury's magnetic field from MESSENGER and BepiColombo as well as through investigations on Mercury's lower mantle temperature heterogeneity and buoyancy forcing in Mercury's core.

1. Introduction

Among the eight solar system planets, six have large-scale intrinsic magnetic fields. These large-scale magnetic fields can be classified into three groups in terms of morphology. The first group is axial-dominant, dipolar, and equatorially symmetric and includes the fields of Earth, Jupiter, and Saturn [*Finlay et al.*, 2010; *Connerney*, 1993; *Yu et al.*, 2010; *Cao et al.*, 2011, 2012]; the second group is nonaxial and multipolar and includes the fields of Uranus and Neptune [*Connerney*, 1993]; a newly recognized group is axial-dominant, dipolar, and equatorially asymmetric and is exemplified by the field of Mercury [*Anderson et al.*, 2011, 2012; *Winslow et al.*, 2014]. MErcury Surface, Space ENvironment, GEochemistry, and Ranging (MESSENGER) magnetometer measurements unambiguously determined northward displacements of the magnetic equator by 0.2 Mercury radii (where 1 Mercury radius is 2440 km) both near the planet and in the distant magnetotail [*Anderson et al.*, 2011, 2012]. This offset of the magnetic equator indicates a strong axial quadrupole component that amounts to 40% of the axial dipole on the surface of the planet and the field strength in the Northern Hemisphere being 3 times that in the Southern Hemisphere (Figure 1a). MESSENGER also confirmed that Mercury's field is relatively weak with a surface field strength that is only 1% of that of the Earth [*Anderson et al.*, 2011, 2012]. Several distinct dynamo models with different ingredients have been proposed for Mercury [*Heimpel et al.*, 2005; *Stanley et al.*, 2005; *Christensen*, 2006; *Wicht et al.*, 2007; *Vilim et al.*, 2010; *Manglik et al.*, 2010; *Heyner et al.*, 2011; *Schubert and Soderlund*, 2011]. The major effort of these models is to reproduce the weak intensity of Mercury's observed magnetic field. However, none of these models generate a quasi-stationary and axial-dominant, yet equatorially asymmetric, magnetic field.

Mercury's iron core is relatively large, occupying the inner 85% of the planet's radius, leaving only the outermost 15% of the planet's radius for the silicate mantle [*Smith et al.*, 2012; *Hauck et al.*, 2013]. The iron core is at least partially liquid [*Margot et al.*, 2007], but the size of a solid inner part is highly uncertain [*Dumberry*, 2011; *Hauck et al.*, 2013]. Recent structural and thermal evolution models, however, suggest that a relatively small inner core is more probable [*Hauck et al.*, 2013; *Tosi et al.*, 2013]. The low iron and high sulfur abundance at Mercury's surface as observed by MESSENGER's X-Ray Spectrometer [*Nittler et al.*, 2011] and Gamma Ray Spectrometer [*Evans et al.*, 2012] is consistent with Mercury forming from highly reduced components [*Zolotov et al.*, 2013]. This redox state would have favored the partitioning of silicon,

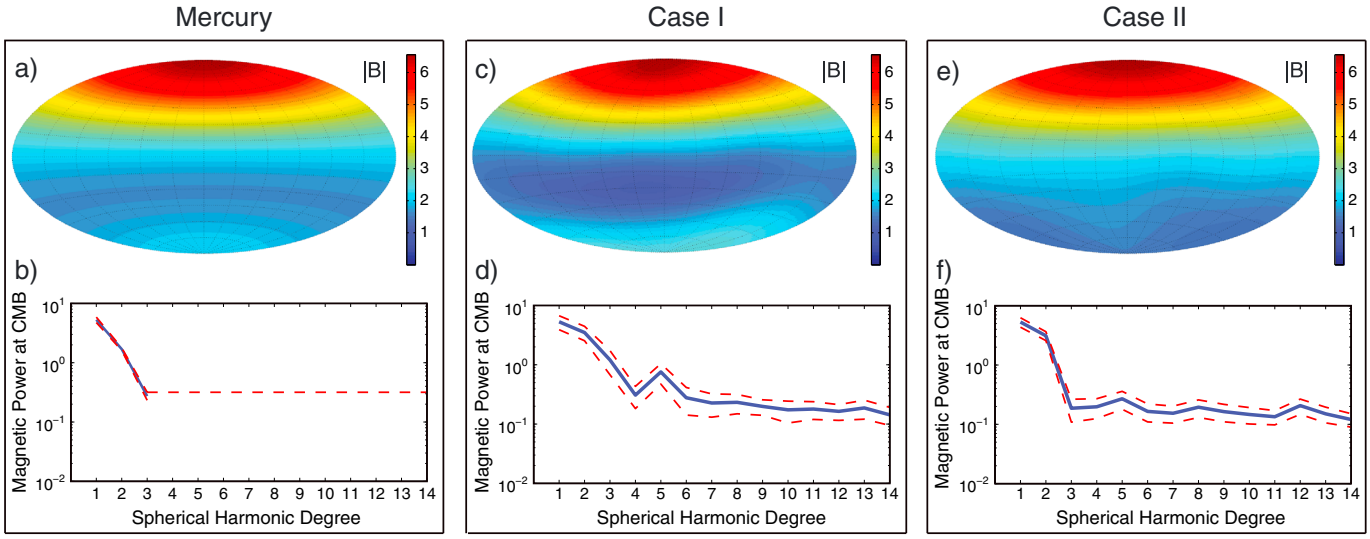

Figure 1. Magnetic field intensity maps and magnetic power spectra of Mercury and our numerical dynamo cases I and II. (a, c, e) Magnetic field intensity maps up to degree and order 3 at the core-mantle boundary (CMB) of Mercury and our numerical dynamo models, respectively. (b, d, f) The corresponding magnetic power spectra up to degree 14. Observed and simulated magnetic fields are nondimensionalized such that the dipole moments equal to 1. The amplitude of the magnetic power spectrum at a given degree n and radius r outside the dynamo region is defined as $A_n = \sum_{m=0}^{n}(n+1)(R_p/r)^{(2n+4)}[(g_n^m)^2 + (h_n^m)^2]$, where R_p is the radius of the planet, g_n^m and h_n^m are Gauss coefficients of degree n and order m at the planet surface. In Figures 1b, 1d, and 1f, blue lines show the mean value while red dashed lines show the 1σ error bar. Magnetic moments of degree and order greater than 3 for Mercury are not determinable from available observations yet; thus, only upper limits are shown. This data-model comparison demonstrates the capability of our dynamo models to reproduce the observed north-south asymmetry, dipole-quadrupole dominance, and axisymmetry of Mercury's magnetic field.

and possibly sulfur, into Mercury's iron core during core-mantle differentiation [*Malavergne et al.*, 2010]. Thus, Mercury's core is likely a Fe-S-Si ternary system rather than a Fe-S system such as the Earth's core. In addition to the possible (double) iron snow scenario in a Fe-S system [*Chen et al.*, 2008] and the classical Earth-like bottom-up inner core growth scenario, the additional complexity in composition can lead to more possibilities of buoyancy forcing modes for Mercury's core dynamo [*Sanloup and Fei*, 2004; *Morard and Katsura*, 2010].

Dynamo action in the cores of terrestrial planets are controlled by the overlying mantles in two primary ways: heat escape from the core is limited by the maximum heat transfer efficiency of the mantle, and lower mantle temperature variations prescribe the spatial heat flow heterogeneity at the core-mantle boundary (CMB). A north-south asymmetric lower mantle temperature field can naturally lead to a north-south asymmetric magnetic field [*Stanley et al.*, 2008; *Aurnou and Aubert*, 2011; *Dietrich and Wicht*, 2013]. Such a north-south asymmetric lower mantle temperature heterogeneity seems to be an option for Mars [*Harder and Christensen*, 1996; *Roberts and Zhong*, 2006] but is unlikely for Mercury. Neither the phase transition nor the substantial viscosity jump evoked to explain a large-scale mantle convection pattern in Mars is likely to exist in Mercury's thin mantle. Considering exogenic origin, *Roberts and Barnouin* [2012] found that the effect on the lower mantle temperature fields from a giant impact similar to the Caloris impact, which formed the largest known impact basin on Mercury, has a characteristic decay time of ~ 30 Myr. This decay time is significantly shorter than the time span between the present and the late heavy bombardment. Thus, any exogenic origin of lower mantle temperature heterogeneity is unlikely to persist to present.

With no evidence for a north-south asymmetry in Mercury's mantle, we pose the following questions. (1) In a planetary dynamo model with equatorially symmetric thermal boundary conditions, can a quasi-stationary Mercury-like magnetic field (axial-dominant, dipolar, and equatorially asymmetric) be generated? (2) What are the mechanisms and conditions necessary for driving such dynamos? In general, symmetry breakings in fluid dynamical systems are well known [cf. *Crawford and Knobloch*, 1991]. Here we are seeking equatorial symmetry breakings in the planetary dynamo realm. In section 2, we present the numerical setup of our planetary dynamo model. In section 3, we present the magnetic fields and flow dynamics in the dynamo models. Finally, we discuss the implications of our results and compare our findings to previously published hemispherical dynamo models.

Table 1. Nondimensional Parameters, Buoyancy Forcing, CMB Heat Flow, Equatorial Symmetry of the Magnetic Fields, and Stability of Eight Selected Numerical Dynamo Cases[a]

	Ra	Pm	Buoyancy Forcing	CMB Heat Flow	Equatorial Symmetry	Stability
Case I	3×10^7	3	VB	Homogeneous	Asym	Bistable
Case II	4×10^7	0.5	VB	$-Y_2^0$, 25%	Asym	Stable
Case III	4×10^7	2	BD	Homogeneous	Sym	Stable
Case IV	4×10^7	2	BD	$-Y_2^0$, 25%	Sym	Stable
Case V	4×10^7	2	VB	Homogeneous	Sym	Stable
Case VI	4×10^7	2	VB	$+Y_2^0$, 25%	Sym	Stable
Case VII	4×10^7	2	VB	$-Y_4^0$, 25%	Asym	Stable
Case VIII	4×10^7	2	VB	$+Y_4^0$, 25%	Sym	Stable

[a]Definitions of the nondimensional parameters can be found in the supporting information. In all eight cases, $E = 1 \times 10^{-4}$, $Pr = 1$, and $\xi = 0.2$. For buoyancy forcing, VB represents volumetric buoyancy in which buoyancy sources are distributed within the entire volume, while BD represents bottom driven in which buoyancy sources are concentrated near the inner boundary.

2. Numerical Dynamo Model

We perform a series of numerical dynamo calculations to explore the role of buoyancy forcing and lower mantle temperature heterogeneity on the core dynamo of Mercury. The numerical dynamo code MagIC [*Wicht*, 2002; *Christensen and Wicht*, 2007] version 3.44 is employed to conduct the numerical experiments in this study. A codensity approach [*Braginsky and Roberts*, 1995; *Wicht and Tilgner*, 2010] is adopted to model thermal-chemical convection in Mercury's liquid core. The nondimensionalized MHD dynamo equations and the numerical setup can be found in the supporting information. Table 1 lists the nondimensional parameters of the simulations presented in this paper.

To capture the range of possible buoyancy forcing modes within Mercury's core, two end-member models are considered: the first is volumetric buoyancy (VB) in which buoyancy sources are distributed within the entire volume, and the second is bottom driven (BD) in which buoyancy sources are concentrated near the inner boundary. Codensity flux conditions are applied at both the inner core boundary (ICB) and core-mantle boundary (CMB) and are calculated differently for volumetric buoyancy cases and bottom driven cases. For volumetric buoyancy cases with uniform buoyancy source ϵ, the CMB codensity flux Q_{CMB} equals $\frac{4}{3}\pi {r_o}^3 \epsilon$ and the ICB codensity flux Q_{ICB} equals $\frac{4}{3}\pi {r_i}^3 \epsilon$, where r_o and r_i are the outer and inner core radii, respectively. The net heat loss from the outer core is balanced by the buoyancy production in the volume: $Q_{\mathrm{CMB}} - Q_{\mathrm{ICB}} = \frac{4}{3}\pi \left(r_o^3 - r_i^3\right) \epsilon$. Q_{ICB} is chosen to reflect a homogeneous cooling of the planet. For bottom driven cases, $\epsilon = 0$ and $Q_{\mathrm{CMB}} = Q_{\mathrm{ICB}}$.

To explore the influence of Mercury's lower mantle temperature heterogeneity on the core dynamo, heterogeneous CMB heat flow patterns that maintain equatorial symmetry are applied in our numerical experiments in addition to a homogeneous CMB heat flow pattern. The heterogeneity of the CMB heat flow is characterized by $q^* = \frac{(q_{\mathrm{max}} - q_{\mathrm{min}})}{2q_{\mathrm{mean}}}$ where q_{max}, q_{min}, and q_{mean} stand for the maximum, minimum, and mean CMB heat flow intensity, respectively. Two different groups of CMB heat flows have been applied: the first group features excess equatorial heat flows while the second group features depleted equatorial heat flows. For each group, both spherical harmonic degree-2 and degree-4 variations have been applied as shown in Figure S1 in the supporting information.

3. Magnetic Fields and Flow Dynamics in Our Dynamo Models

Figure 1 compares MESSENGER observations of Mercury's magnetic field with two of our numerical dynamo cases powered by volumetric buoyancy. Homogeneous CMB heat flow is applied in case I, while 25% degree-2 excess equatorial CMB heat flow is applied in case II. The magnetic field intensity maps and the magnetic power spectra are shown on the surface of the dynamo region for both observations and simulations. In the observations and two simulation cases presented in Figure 1, the magnetic fields are axially aligned with significant north-south asymmetry; the magnetic power spectra are dipole-quadrupole dominant with little contributions from other harmonic degrees. Figure 2 shows the stability and axisymmetry of the magnetic fields in case II: the magnetic equator offset reaches a quasi-steady state within one magnetic diffusion time and stays stable for the rest of the simulation; contributions from the

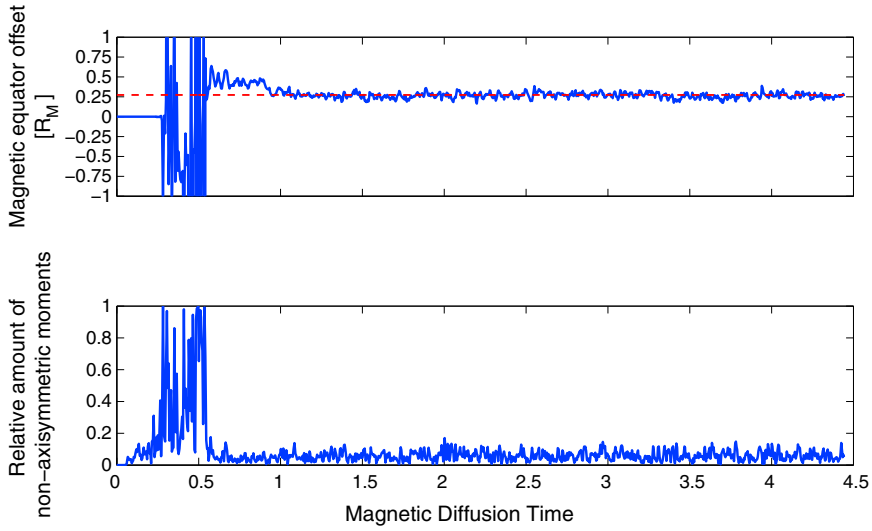

Figure 2. Stability and axisymmetry of the asymmetric magnetic fields in our numerical dynamo case II. (top) The stability of the solution. After the initial transit behavior, the magnetic field is nonreversing for over four magnetic diffusion times and the offset of the magnetic equator is nearly constant ($0.26 \pm 0.03\ R_P$ with the dynamo surface assumed to be at $0.85\ R_P$) between $t = 1$ and 4.45 magnetic diffusion times. One magnetic diffusion time for Mercury is on the order of 10, 000 Earth years. (bottom) The axisymmetry of the dynamo solution. The relative strength of the nonaxisymmetric magnetic moments remains within 10% from $t = 1$ to 4.45 magnetic diffusion times.

nonaxisymmetric magnetic moments remain within 10% once the steady state is reached. Our numerical modeling results demonstrate that planetary dynamo systems with equatorially symmetric thermal boundaries are capable of reproducing the observed equatorial symmetry breaking of Mercury's magnetic field and that quasi-steady solutions can be maintained. The equatorial symmetry breaking in our dynamo model has no a priori preference of north or south; however, stronger magnetic fields remain in one hemisphere (e.g., north) once that particular symmetry breaking is established.

Table 1 summarizes selected numerical dynamo cases with different buoyancy forcing and CMB heat flow patterns. The setups of the two cases presented in Figure 1 are representative of those producing quasi-stationary Mercury-like magnetic fields: volumetric buoyancy is a key ingredient for the equatorial symmetry breaking, while local equatorial excess CMB heat flows help to promote and stabilize such solutions. In our numerical studies, solutions featuring equatorially asymmetric magnetic fields emerge with homogeneous CMB heat flows (e.g., case I). However, equatorially asymmetric magnetic fields with homogeneous CMB heat flows are typically highly time dependent and have strong nonaxisymmetric contributions. We found that applying local equatorial excess CMB heat flow (e.g., cases II and VII) not only promotes but also stabilizes such equatorial symmetry breaking (e.g., Figure 2). In contrast, local-depleted CMB heat flow near the equator (e.g., cases VI and VIII) suppresses quasi-steady equatorial symmetry breakings in general. It is also important to emphasize that volumetric buoyancy does not guarantee equatorial symmetry breaking, since such symmetry breaking occurs only at intermediate Rayleigh number. With volumetric buoyancy, we find that Earth-like magnetic fields can be reached at low Rayleigh numbers while Uranus-Neptune-like magnetic fields can be reached at high Rayleigh numbers. In bottom driven cases with equatorially symmetric thermal boundaries (e.g., cases III and IV), no quasi-steady equatorial symmetry breaking has been identified.

The flow fields that generate the equatorially asymmetric magnetic field in case II are shown, via three-dimensional renderings, in Figure 3. Figure 3a displays the velocity component U_Z that is parallel to the spin axis. There is a significant equatorial asymmetry in the z component of the velocity field, with stronger U_Z in the Northern Hemisphere than in the Southern Hemisphere. Figure 3b displays ω_Z, the z component of the flow vorticity defined as $\omega_Z = (\vec{\nabla} \times \vec{U})_Z$. Less significant equatorial asymmetry exists in the z vorticity. The combination of z vorticity and z velocity plays an important role in the dynamo process [cf. *Moffatt*, 1978; *Krause and Rädler*, 1980; *Jones*, 2011]. Kinetic helicity, defined as $H = \vec{U} \cdot (\vec{\nabla} \times \vec{U})$, has been frequently used to quantify this effect. Figure 3c shows the axial helicity, $H_Z = U_Z \cdot (\vec{\nabla} \times \vec{U})_Z$, which is much stronger in the Northern than in the Southern Hemisphere owing mostly to the strong asymmetry in the z

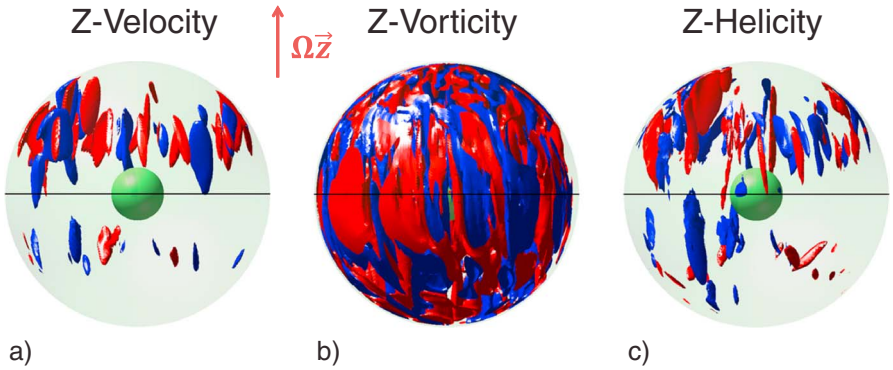

Figure 3. Flow structures in our dynamo case II. The *z* components of (a) velocity, (b) vorticity, and (c) helicity are shown via three-dimensional rendering with red (blue) colors corresponding to positive (negative) values in each quantity. It can be seen that the *z* velocity displays significant hemispherical asymmetry, while the *z* vorticity shows less significant hemispherical asymmetry. The combination of the two leads to the difference in helicity between the Northern and Southern Hemispheres (root-mean-square axial helicity in the Northern Hemisphere is about twice that in the Southern Hemisphere). Boundary layers have been excluded in all renderings and calculations of velocity, vorticity, and helicity.

component of the flow. This explains why the magnetic field is much stronger in the Northern than in the Southern Hemisphere. The ability to create flows with different kinetic helicity amplitudes in the two hemispheres while maintaining similar heat transfer efficiencies is the key to generating asymmetric magnetic fields with symmetric thermal boundaries. Zonal flow and zonal magnetic fields in case II are compared to those in case V in Figure S2 in the supporting information.

Equatorially symmetric and antisymmetric convective modes form two distinct solution families in rapidly rotating spheres or spherical shells. Both modes are organized as relatively small scale cylindrical columns aligned parallel to the spin axis (e.g., Figure 3). The one with equatorially mirror-symmetric U_Z is referred to as the even mode [*Busse*, 1970] and the one with equatorially antisymmetric U_Z is referred to as the odd mode [*Roberts*, 1968] as sketched in Figure 4. The nonaxisymmetric even mode is most unstable, regardless of how the buoyancy sources are distributed and are the classical convective columns [*Busse*, 1970; *Jones et al.*, 2009]. The nonaxisymmetric odd mode has been predicted to also exist given modest forcing [*Jones et al.*, 2009; *Calkins et al.*, 2013] but has not been reported in previous self-consistent three-dimensional dynamo simulations (cf. only the axisymmetric odd mode has been clearly identified and reported by *Landeau and Aubert* [2011]). Linear superposition of even and odd modes will naturally give rise to asymmetric U_Z, ω_Z, and H_Z in the north and south as illustrated in Figure 4, which can serve as the first-order physical model for the flow structures in our hemispherical dynamo models. Volumetric buoyancy and local equatorial excess CMB heat flow seem to lower the critical Rayleigh number for the onset of the nonaxisymmetric odd mode and/or to promote a similar azimuthal wave number for the nonaxisymmetric even and odd modes via nonlinear interaction.

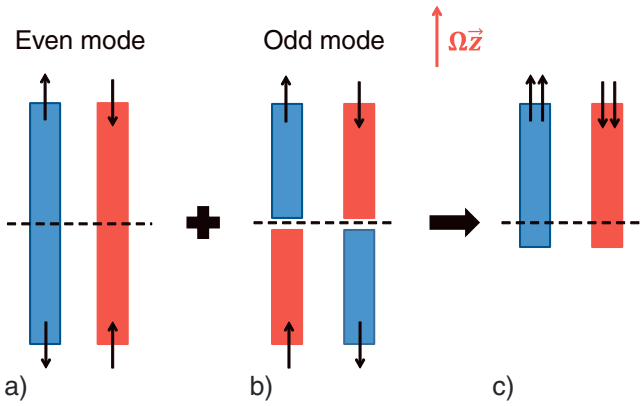

Figure 4. Sketches of the two dominant modes of columnar convection that arise in rapidly rotating spheres and spherical shells. (a) The nonaxisymmetric even mode [*Busse*, 1970], (b) the nonaxisymmetric odd mode [*Roberts*, 1968], and (c) the linear superposition of the two modes. In this illustration, thin black arrows represent *z* flow, red (blue) color blocks represent positive (negative) *z*-vorticity, thin black dashed lines represent the equator, and the red arrow represents the planetary spin axis.

When measured using the conventionally defined Elsasser number, the mean CMB magnetic field strength in our dynamo cases I and II are as weak as 3×10^{-2}. The Elsasser number is defined here as $\Lambda = \frac{\sigma B^2}{\rho\Omega}$, where σ is the electrical conductivity of the outer core, B is the magnetic field strength, ρ is the fluid density of the outer core, and Ω is the rotation rate of the mantle

[*Chandrasekhar*, 1961; *Christensen*, 2010; *Soderlund et al.*, 2012]. The field is much weaker than in typical dynamo solutions with Elsasser number of order unity and is thus closer to Mercury's anomalously weak field. Importantly, any additional effect such as electromagnetic filtering [*Christensen*, 2006] by a solid or stably stratified Fe-S layer at the top of the dynamo region or solar wind feedback [*Heyner et al.*, 2011] will likely further lower the simulated magnetic field strength.

4. Summary and Discussion

Hemispherical dynamo models have been studied in different contexts, with application to the Sun [*Grote and Busse*, 2000] and Mars [*Stanley et al.*, 2008; *Landeau and Aubert*, 2011; *Dietrich and Wicht*, 2013]. *Stanley et al.* [2008] and *Dietrich and Wicht* [2013] both employed a degree-1 north-south asymmetric CMB heat flow heterogeneity and thus are unlikely to be applicable to Mercury. The magnetic fields in *Grote and Busse* [2000] typically feature chaotic time dependence and contain substantial contributions from the nonaxisymmetric components, reducing the applicability to Mercury. *Landeau and Aubert* [2011] explored homogeneous CMB heat flows only and interpret the symmetry breaking in their results as a result of the axisymmetric odd mode. Based on the information provided in *Landeau and Aubert* [2011], it is difficult to assess whether the equatorially asymmetric magnetic field in their dynamo models is stable and axisymmetric, given our finding that such stable solutions are extremely rare with homogeneous CMB heat flows.

We have shown that quasi-stationary Mercury-like magnetic fields (axial-dominant, dipolar, and equatorially asymmetric) can be generated even with equatorially symmetric thermal boundary conditions. The equatorial symmetry breaking in the dynamo-generated magnetic fields reflects the asymmetric kinetic helicity resulting from mutual excitation of two fundamental modes of columnar convection in rapidly rotating spherical shells. The ingredients to promote such symmetry breaking include volumetric buoyancy and local excess equatorial CMB heat flow. This implies that, unlike the Earth's dynamo which is mainly powered by light element expulsion and latent heat release associated with inner core growth, Mercury's dynamo is likely powered by uniformly distributed buoyancy sources within the liquid core. The different driving mode could be explained by the additional complexities of the Fe-S-Si system under the pressure and temperature of Mercury's core. Even in a Fe-S core, the (double) iron snow scenario [*Chen et al.*, 2008] and the exsolution of light elements [*Stevenson*, 1983] can provide forcing scenarios comparable to volumetrically distributed buoyancy sources. Insight into the buoyancy forcing within Mercury's core will come from future laboratory and numerical investigations in the equation of state of the Fe-S-Si system. As to the CMB heat flow pattern, our dynamo model favors local excess heat flow out of Mercury's core near the equator. Whether such a pattern exists at the CMB of Mercury can be tested with 3-D mantle convection models constrained by MESSENGER observations. As to the inner core size, we have tested different inner core sizes with $\frac{r_{ICB}}{r_{CMB}}$ that range from 0.2 to 0.75. Given that volumetric buoyancy is the driving mode and local excess equatorial CMB heat flow is applied, equatorial symmetry breaking occurs with all inner core sizes tested. However, quasi-steady dipole-quadrupole dominant solutions have only been reached with $\frac{r_{ICB}}{r_{CMB}}$ smaller than 0.50. Thus, our dynamo model favors a small inner core inside Mercury, consistent with recent structural and evolution models [*Hauck et al.*, 2013; *Tosi et al.*, 2013; *Grott et al.*, 2011]. Gravity, topography, temperature, and heat flow measurements from future missions (e.g., BepiColombo) will further advance our understanding of Mercury's mantle and core and can be used to test the predictions of our dynamo models.

Acknowledgments

Computational resources were provided by the NASA High-End Computing (HEC) Program through the NASA Advanced Supercomputing (NAS) Division at Ames Research Center. H. Cao gratefully acknowledges support from the visitors grant by the Max Planck Institute for Solar System Research. J.M. Aurnou gratefully acknowledges the NSF Geophysics Program for support. W. Dietrich and J. Wicht were supported by the Helmholtz Alliance "Planetary Evolution and Life." K.M. Soderlund gratefully acknowledges funding supports from the National Science Foundation (grant AST-0909206) and the Institute for Geophysics of the Jackson School of Geosciences at the University of Texas at Austin (UTIG). The authors thank the referees for their valuable comments and suggestions.

The Editor thanks two anonymous reviewers for their assistance in evaluating this paper.

References

Anderson, B. J., C. L. Johnson, H. Korth, M. E. Purucker, R. M. Winslow, J. A. Slavin, S. C. Solomon, R. L. McNutt, J. M. Raines, and T. H. Zurbuchen (2011), The global magnetic field of Mercury from MESSENGER orbital observations, *Science*, *333*, 1859–1862, doi:10.1126/science.1211001.

Anderson, B. J., C. L. Johnson, H. Korth, R. M. Winslow, J. E. Borovsky, M. E. Purucker, J. A. Slavin, S. C. Solomon, M. T. Zuber, and R. L. McNutt Jr. (2012), Low-degree structure in Mercury's planetary magnetic field, *J. Geophys. Res.*, *117*, E00L12, doi:10.1029/2012JE004159.

Aurnou, J. M., and J. Aubert (2011), End-member models of boundary-modulated convective dynamos, *Phys. Earth Planet. Inter.*, *187*, 353–363, doi:10.1016/j.pepi.2011.05.011.

Braginsky, S. I., and P. H. Roberts (1995), Equations governing convection in Earth's core and the geodynamo, *Geophys. Astrophys. Fluid Dyn.*, *79*, 1–97, doi:10.1080/03091929508228992.

Busse, F. H. (1970), Thermal instabilities in rapidly rotating systems, *J. Fluid Mech.*, *44*, 441–460, doi:10.1017/S0022112070001921.

Calkins, M. A., K. Julien, and P. Marti (2013), Three-dimensional quasi-geostrophic convection in the rotating cylindrical annulus with steeply sloping endwalls, *J. Fluid Mech.*, *732*, 214–244, doi:10.1017/jfm.2013.309.

Cao, H., C. T. Russell, U. R. Christensen, M. K. Dougherty, and M. E. Burton (2011), Saturn's very axisymmetric magnetic field: No detectable secular variation or tilt, *Earth Planet. Sci. Lett.*, *304*, 22–28, doi:10.1016/j.epsl.2011.02.035.

Cao, H., C. T. Russell, J. Wicht, U. R. Christensen, and M. K. Dougherty (2012), Saturn's high degree magnetic moments: Evidence for a unique planetary dynamo, *Icarus*, *221*, 388–394, doi:10.1016/j.icarus.2012.08.007.

Chandrasekhar, S. (1961), *Hydrodynamic and Hydromagnetic Stability*, Oxford Univ. Press, Oxford, U. K.

Chen, B., J. Li, and S. A. Hauck (2008), Non-ideal liquidus curve in the Fe-S system and Mercury's snowing core, *Geophys. Res. Lett.*, *35*, L07201, doi:10.1029/2008GL033311.

Christensen, U., and J. Wicht (2007), Numerical dynamo simulations, in *Treatise on Geophysics*, edited by G. Schubert, pp. 245–282, Elsevier, Amsterdam, Netherlands, doi:10.1016/B978-044452748-6.00134-6.

Christensen, U. R. (2006), A deep dynamo generating Mercury's magnetic field, *Nature*, *444*, 1056–1058, doi:10.1038/nature05342.

Christensen, U. R. (2010), Dynamo scaling laws and applications to the planets, *Space Sci. Rev.*, *152*, 565–590, doi:10.1007/s11214-009-9553-2.

Connerney, J. E. P. (1993), Magnetic fields of the outer planets, *J. Geophys. Res.*, *98*, 18,659–18,679, doi:10.1029/93JE00980.

Crawford, J. D., and E. Knobloch (1991), Symmetry and symmetry-breaking bifurcations in fluid dynamics, *Annu. Rev. Fluid Mech.*, *23*, 341–387, doi:10.1146/annurev.fl.23.010191.002013.

Dietrich, W., and J. Wicht (2013), A hemispherical dynamo model: Implications for the Martian crustal magnetization, *Phys. Earth Planet. Inter.*, *217*, 10–21, doi:10.1016/j.pepi.2013.01.001.

Dumberry, M. (2011), The free librations of Mercury and the size of its inner core, *Geophys. Res. Lett.*, *38*, L16202, doi:10.1029/2011GL048277.

Evans, L. G., et al. (2012), Major-element abundances on the surface of Mercury: Results from the MESSENGER Gamma-Ray Spectrometer, *J. Geophys. Res.*, *117*, E00L07, doi:10.1029/2012JE004178.

Finlay, C. C., et al. (2010), International geomagnetic reference field: The eleventh generation, *Geophys. J. Int.*, *183*, 1216–1230, doi:10.1111/j.1365-246X.2010.04804.x.

Grote, E., and F. H. Busse (2000), Hemispherical dynamos generated by convection in rotating spherical shells, *Phys. Rev. E*, *62*, 4457–4460, doi:10.1103/PhysRevE.62.4457.

Grott, M., D. Breuer, and M. Laneuville (2011), Thermo-chemical evolution and global contraction of Mercury, *Earth Planet. Sci. Lett.*, *307*, 135–146, doi:10.1016/j.epsl.2011.04.040.

Harder, H., and U. R. Christensen (1996), A one-plume model of Martian mantle convection, *Nature*, *380*, 507–509, doi:10.1038/380507a0.

Hauck, S. A., et al. (2013), The curious case of Mercury's internal structure, *J. Geophys. Res. Planets*, *118*, 1204–1220, doi:10.1002/jgre.20091.

Heimpel, M. H., J. M. Aurnou, F. M. Al-Shamali, and N. Gomez Perez (2005), A numerical study of dynamo action as a function of spherical shell geometry, *Earth Planet. Sci. Lett.*, *236*, 542–557, doi:10.1016/j.epsl.2005.04.032.

Heyner, D., J. Wicht, N. Gómez-Pérez, D. Schmitt, H.-U. Auster, and K.-H. Glassmeier (2011), Evidence from numerical experiments for a feedback dynamo generating Mercury's magnetic field, *Science*, *334*, 1690–1693, doi:10.1126/science.1207290.

Jones, C. A. (2011), Planetary magnetic fields and fluid dynamos, *Annu. Rev. Fluid Mech.*, *43*, 583–614, doi:10.1146/annurev-fluid-122109-160727.

Jones, C. A., K. M. Kuzanyan, and R. H. Mitchell (2009), Linear theory of compressible convection in rapidly rotating spherical shells, using the anelastic approximation, *J. Fluid Mech.*, *634*, 291–319, doi:10.1017/S0022112009007253.

Krause, F., and K. H. Rädler (1980), *Mean-Field Magnetohydrodynamics and Dynamo Theory*, Akademie-Verlag, Berlin, Germany. [Available at http://books.google.com/books?id=QJMJAQAAIAAJ.]

Landeau, M., and J. Aubert (2011), Equatorially asymmetric convection inducing a hemispherical magnetic field in rotating spheres and implications for the past Martian dynamo, *Phys. Earth Planet. Inter.*, *185*, 61–73, doi:10.1016/j.pepi.2011.01.004.

Malavergne, V., M. J. Toplis, S. Berthet, and J. Jones (2010), Highly reducing conditions during core formation on Mercury: Implications for internal structure and the origin of a magnetic field, *Icarus*, *206*, 199–209, doi:10.1016/j.icarus.2009.09.001.

Manglik, A., J. Wicht, and U. R. Christensen (2010), A dynamo model with double diffusive convection for Mercury's core, *Earth Planet. Sci. Lett.*, *289*, 619–628, doi:10.1016/j.epsl.2009.12.007.

Margot, J. L., S. J. Peale, R. F. Jurgens, M. A. Slade, and I. V. Holin (2007), Large longitude libration of Mercury reveals a molten core, *Science*, *316*, 710–714, doi:10.1126/science.1140514.

Moffatt, H. K. (1978), *Magnetic Field Generation in Electrically Conducting Fluids*, p. 353, Cambridge Univ. Press, Cambridge, U. K.

Morard, G., and T. Katsura (2010), Pressure-temperature cartography of Fe-S-Si immiscible system, *Geochim. Cosmochim. Acta*, *74*, 3659–3667, doi:10.1016/j.gca.2010.03.025.

Nittler, L. R., et al. (2011), The major-element composition of Mercury's surface from MESSENGER X-ray spectrometry, *Science*, *333*, 1847–1850, doi:10.1126/science.1211567.

Roberts, J. H., and O. S. Barnouin (2012), The effect of the Caloris impact on the mantle dynamics and volcanism of Mercury, *J. Geophys. Res.*, *117*, E02007, doi:10.1029/2011JE003876.

Roberts, J. H., and S. Zhong (2006), Degree-1 convection in the Martian mantle and the origin of the hemispheric dichotomy, *J. Geophys. Res.*, *111*, E06013, doi:10.1029/2005JE002668.

Roberts, P. H. (1968), On the thermal instability of a rotating-fluid sphere containing heat sources, *R. Soc. London Philos. Trans. Ser. A*, *263*, 93–117, doi:10.1098/rsta.1968.0007.

Sanloup, C., and Y. Fei (2004), Closure of the Fe-S-Si liquid miscibility gap at high pressure, *Phys. Earth Planet. Inter.*, *147*, 57–65, doi:10.1016/j.pepi.2004.06.008.

Schubert, G., and K. M. Soderlund (2011), Planetary magnetic fields: Observations and models, *Phys. Earth Planet. Inter.*, *187*, 92–108, doi:10.1016/j.pepi.2011.05.013.

Smith, D. E., et al. (2012), Gravity field and internal structure of Mercury from MESSENGER, *Science*, *336*, 214–217, doi:10.1126/science.1218809.

Soderlund, K. M., E. M. King, and J. M. Aurnou (2012), The influence of magnetic fields in planetary dynamo models, *Earth Planet. Sci. Lett.*, *333*, 9–20, doi:10.1016/j.epsl.2012.03.038.

Stanley, S., J. Bloxham, W. E. Hutchison, and M. T. Zuber (2005), Thin shell dynamo models consistent with Mercury's weak observed magnetic field [rapid communication], *Earth Planet. Sci. Lett.*, *234*, 27–38, doi:10.1016/j.epsl.2005.02.040.

Stanley, S., L. Elkins-Tanton, M. T. Zuber, and E. M. Parmentier (2008), Mars' paleomagnetic field as the result of a single-hemisphere dynamo, *Science*, *321*, 1822–1825, doi:10.1126/science.1161119.

Stevenson, D. J. (1983), Planetary magnetic fields, *Rep. Prog. Phys.*, *46*, 555–557, doi:10.1088/0034-4885/46/5/001.

Tosi, N., M. Grott, A.-C. Plesa, and D. Breuer (2013), Thermochemical evolution of Mercury's interior, *J. Geophys. Res. Planets*, *118*, 1–14, doi:10.1002/jgre.20168.

Vilim, R., S. Stanley, and S. A. Hauck (2010), Iron snow zones as a mechanism for generating Mercury's weak observed magnetic field, *J. Geophys. Res.*, *115*, E11003, doi:10.1029/2009JE003528.

Wicht, J. (2002), Inner-core conductivity in numerical dynamo simulations, *Phys. Earth Planet. Inter.*, *132*, 281–302, doi:10.1016/S0031-9201(02)00078-X.

Wicht, J., and A. Tilgner (2010), Theory and modeling of planetary dynamos, *Space Sci. Rev.*, *152*, 501–542, doi:10.1007/s11214-010-9638-y.

Wicht, J., M. Mandea, F. Takahashi, U. R. Christensen, M. Matsushima, and B. Langlais (2007), The origin of Mercury's internal magnetic field, *Space Sci. Rev.*, *132*, 261–290, doi:10.1007/s11214-007-9280-5.

Winslow, R. M., et al. (2014), Mercury's surface magnetic field determined from proton-reflection magnetometry, *Geophys. Res. Lett.*, 1944–8007, doi:10.1002/2014GL060258.

Yu, Z. J., H. K. Leinweber, and C. T. Russell (2010), Galileo constraints on the secular variation of the Jovian magnetic field, *J. Geophys. Res.*, *115*, E03002, doi:10.1029/2009JE003492.

Zolotov, M. Y., A. L. Sprague, S. A. Hauck, L. R. Nittler, S. C. Solomon, and S. Z. Weider (2013), The redox state, FeO content, and origin of sulfur-rich magmas on Mercury, *J. Geophys. Res. Planets*, *118*, 138–146, doi:10.1029/2012JE004274.

implants that require only intermittent power. Those can include devices to stimulate nerve-cell clusters called ganglia to relieve pain (their first human trial will be on ganglion stimulation) and sensors to monitor various biological functions. Miniature pacemakers are a possibility, too, though they'd need to include an onboard rechargeable battery. But because that battery need only carry enough power to last weeks, rather than years, it can be made small.

Johanna Miller

References

1. J. S. Ho et al., *Proc. Natl. Acad. Sci. USA* **111**, 7974 (2014).
2. S. Kim, J. S. Ho, A. S. Y. Poon, *Phys. Rev. Lett.* **110**, 203905 (2013).

Model dynamo may solve Mercury mystery

Simulations suggest that the planet's top-heavy magnetic field derives from the unusual chemistry of its core.

In March 2011, nearly seven years after its launch, NASA's *MESSENGER* probe became the first manmade object to orbit Mercury, where it began a detailed survey of the planet's geochemistry, topography, and space environment. (See the article by Sean Solomon, PHYSICS TODAY, January 2011, page 50.) Within a few months, the spacecraft delivered a surprise: Mercury's magnetic field is top heavy—three times as strong at the north pole as it is at the south pole.[1]

Of the planets in our solar system that possess a global, dipolar magnetic field, only Mercury exhibits the north–south asymmetry. The finding is all the more puzzling because by most every other measure, including gravitational field strength and surface temperature, Mercury's northern and southern halves are essentially identical. Now, with new insights from simulations of the planet's dynamo—the turbulent, magnetic-field-inducing flow of molten material in the planet's core—Hao Cao, Christopher Russell (both at UCLA), and coworkers think they've uncovered the recipe for the symmetry breaking that gave Mercury its unique magnetic field.[2]

Uncommon core

Planetary dynamos feed on motion. As molten metal churns in the core, it stretches and bends existing magnetic field lines, thereby inducing additional magnetic field. If the motion were to stop, the planet's field would decay and vanish. (See the article by Daniel Lathrop and Cary Forest, PHYSICS TODAY, July 2011, page 40.)

In Earth's dynamo, core flows are thought to be sustained partly with energy supplied by phase changes at the interface between the solid inner core and the fluid outer core (see figure 1a). As the planet cools, the inner core grows; it incorporates iron and other heavy elements from the outer core and leaves behind a fluid rich in low-density elements such as sulfur. That hot, buoyant fluid rises to the overlying mantle and generates the convective motion that powers the dynamo. (See the article by Peter Olson, PHYSICS TODAY, November 2013, page 30.)

Traditionally, Mercury's dynamo has been assumed to operate in similar fashion. But there are reasons to suspect that convective forcing in Mercury's core may be significantly more complex than it is in Earth's. For starters, Mercury's core is thought to contain a much higher concentration of light elements; their depression of the core's freezing point is currently the only viable explanation for why the relatively small core hasn't already frozen completely solid. (See PHYSICS TODAY, July 2007, page 22.)

In 2008 Bin Chen, Jie Li (both then at the University of Illinois at Urbana-Champaign), and Steven Hauck II (Case Western Reserve University, Cleveland, Ohio) showed that when molten iron contains a sufficiently large admixture of sulfur and is compressed to Mercury-like pressures, iron can spontaneously precipitate—even when there's no solid–liquid interface to seed the phase change.[3] They predicted that precipitation could potentially occur in two layers, so-called snow zones, inside Mercury's core. Sources of heavy precipitates and buoyant light elements, the snow zones (depicted in figure 1b) would further stir the dynamo.

Newer assessments of Mercury's geochemistry hint at still more complicated forcing patterns. Spectroscopic measurements indicate that Mercury's silicate surface is poor in iron and rich in sulfur, which suggests that the planet formed under highly reducing chemical conditions. Laboratory experiments mimicking those conditions demonstrate that Mercury's core likely acquired substantial admixtures of both sulfur and silicon as it formed. If so, the liquid part of the core could consist of two immiscible layers—an iron–sulfur phase and an iron–silicon phase—each of which could spawn snow zones and potentially give rise to other exotic phase behavior.

To see how different forcing patterns influence dynamo-generated magnetic fields, Cao and his coworkers teamed with a numerical modelling group led by Johannes Wicht (Max Planck Institute for Solar System Research, Göttingen, Germany). The researchers didn't attempt to simulate every possible scenario, just two extreme cases: An Earth-like scenario in which the dynamo is stirred from below and a so-called vol-

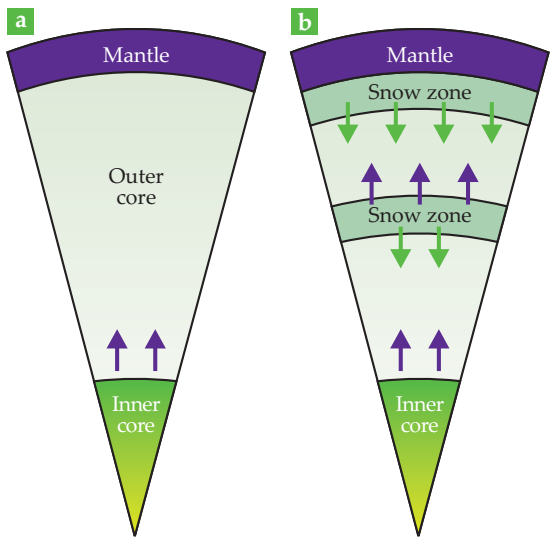

Figure 1. Planetary dynamos are driven in part by convective circulation resulting from phase changes in the planet's interior. **(a)** In Earth, for example, light elements (purple arrows) are expelled into the molten outer core as the solid inner core grows. Those light elements stir the core as they rise to the mantle. **(b)** In Mercury, light elements (purple arrows) and heavy solids (green arrows) can also originate in localized regions of precipitation known as snow zones. (Adapted from ref. 3.)

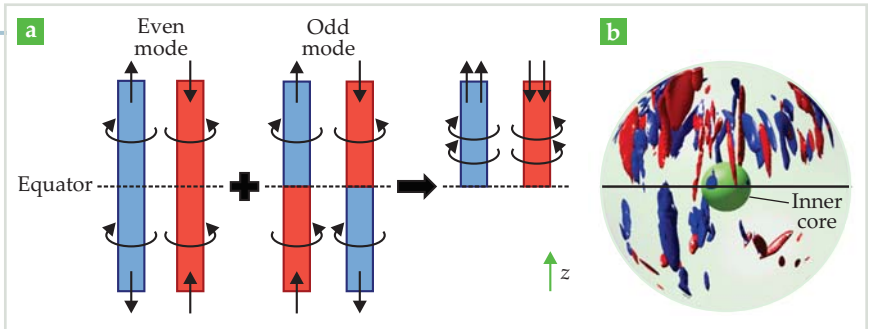

Figure 2. Symmetry breaking in dynamos. **(a)** Interactions between even and odd flow modes in a planetary dynamo tend to enhance flow in one hemisphere and diminish it in the other. (Straight black arrows indicate the velocity component in the direction *z* of the spin axis; curved arrows indicate vorticity.) **(b)** In a dynamo simulation, the interactions between modes manifest as an asymmetry in helicity—a measure of the flow's combined velocity and vorticity. (In both panels, red and blue denote regions of positive and negative vorticity, respectively.) (Adapted from ref. 2.)

umetric buoyancy scenario, which simulates a fully pervasive iron snow. Whereas the Earth-like forcing always yielded a symmetric magnetic field, volumetric buoyancy consistently gave rise to asymmetries similar to that observed for Mercury.

"It's somewhat counterintuitive, because all of the boundary conditions are symmetric; we don't know *a priori* if the system will be stronger in the north or in the south," says Cao. "But once the system chooses a hemisphere, it stays in that state. It's a classic example of spontaneous symmetry breaking."

Odds and evens

Planetary dynamos are generally thought to be organized into helical flows along columns aligned parallel to the spin (*z*) axis. In a typical dynamo, such as Earth's, the flows in neighboring columns are alternately directed toward and away from the equator, as depicted schematically at the left of figure 2a. (Straight black arrows indicate the axial velocity; curved arrows indicate vorticity, a measure of the fluid's spinning motion.) In mathematical parlance, the flow configuration is known as an even mode, since the flows in the northern hemisphere mirror those in the south.

Fluid mechanical theory predicts that under strong forcing, dynamos can also host an odd mode, in which fluid travels through the equator, reversing vorticity along the way. Cao and company noticed that although the odd mode itself does not distinguish between northern and southern hemispheres, its superposition with the even mode does. That superposition provides a possible route to magnetic-field asymmetry. Although the precise structure of the magnetic field depends on complex interactions between the three-dimensional flow and preexisting field lines, the field strength correlates roughly with helicity, the dot product of velocity and vorticity. When the odd and even modes overlap, their superposition enhances helicity in one hemisphere and diminishes it in the other. Indeed, that theoretical picture is consistent with helicity profiles obtained in the team's dynamo simulations, as shown in figure 2b.

The researchers aren't the first to see symmetry breaking in dynamo simulations. Three years ago, Maylis Landeau and Julien Aubert (both then at the University of Paris Diderot) reported a similar magnetic asymmetry in simulations of the ancient Martian dynamo.[4] Landeau and Aubert, however, specifically considered the case of a planet with an all-fluid core; the asymmetry resulted from a particular flow mode in which fluid passes through the center of the planet as it travels between poles. Such a mode is plausible for early Mars but not for planets that, like Mercury, have sizeable solid inner cores.

At first glance, the mechanism that Cao and company propose for Mercury's symmetry breaking seems to contradict previous theoretical studies that predict that the dynamo's columnar flow structure should destabilize before convective forcing becomes strong enough to excite the odd mode. But those studies assume Earth-like forcing, notes Jonathan Aurnou (UCLA), coauthor of the new paper. "The volumetric buoyancy essentially acts to keep the columns stable."

Another facet of the team's model may have been central to symmetry breaking. The researchers tried imposing a variety of boundary conditions for the core's outer edge, including the customary uniform heat-flux condition and less traditional scenarios in which heat escapes faster near the equator

than at mid and high latitudes. Although north–south asymmetries could occur with uniform heat fluxes, the resulting dipoles tended to lie off-center with the spin axis, fluctuate wildly over time, and exhibit a weaker asymmetry than exists on Mercury. When heat was assumed to escape faster near the equators, the fields looked nearly identical to Mercury's.

To some extent, then, the theoretical explanation of Mercury's asymmetry hinges on the unproven assumption that the core cools fastest at the equator, probably by way of enhanced convection in the mantle. According to Sean Solomon, principal investigator of the *MESSENGER* mission, the assumption isn't too far-fetched. "If there were sustained, enhanced upwelling of the mantle in the equatorial zones—and if that pattern persisted over most of Mercury's history—then you might expect to see a thicker crust in the equatorial regions. That is, in fact, what we see."

Solomon cautions, however, that it's not a given that Mercury's mantle is convecting at all—much less that it is removing heat fastest near the equator. "Most but not all Mercury models have mantle convection turning off sometime before the present," he says. "Our ignorance is vast."

Ashley G. Smart

References

1. B. J. Anderson et al., *Science* **333**, 1859 (2011).
2. H. Cao et al., *Geophys. Res. Lett.* (in press).
3. B. Chen, J. Li, S. A. Hauck II, *Geophys. Res. Lett.* **35**, L07201 (2008).
4. M. Landeau, J. Aubert, *Phys. Earth Planet. Inter.* **185**, 61 (2011).

Charged polymers form unusual nanostructures

A hybrid theoretical description provides a roadmap to designing better battery electrolytes.

Diblock copolymers—made up of a chain of monomer A bound to a chain of monomer B, as shown in figure 1a—are of great theoretical and practical interest. When the A and B monomers are sufficiently immiscible, they can segregate into self-assembled periodic nanostructures such as alternating layers or hexagonally ordered rods. The morphology of those two-phase structures depends on the phase immiscibility, the relative lengths of the A and B chains, and other factors. Choosing the A and B phases with complementary properties enables a variety of applications. (See the article by Frank Bates and Glenn Fredrickson, PHYSICS TODAY, February 1999, page 32.)

For example, to make a solid-state electrolyte for a battery or fuel cell, one can optimize the A phase for ionic conductivity, with negative ions bound to the polymer chains balanced by unbound positive ions, and the B phase for mechanical stability. Numerous experiments, however, have shown that the theoretically derived phase diagram that predicts the nanophase morphology no longer applies when one of the phases is charged.[1]

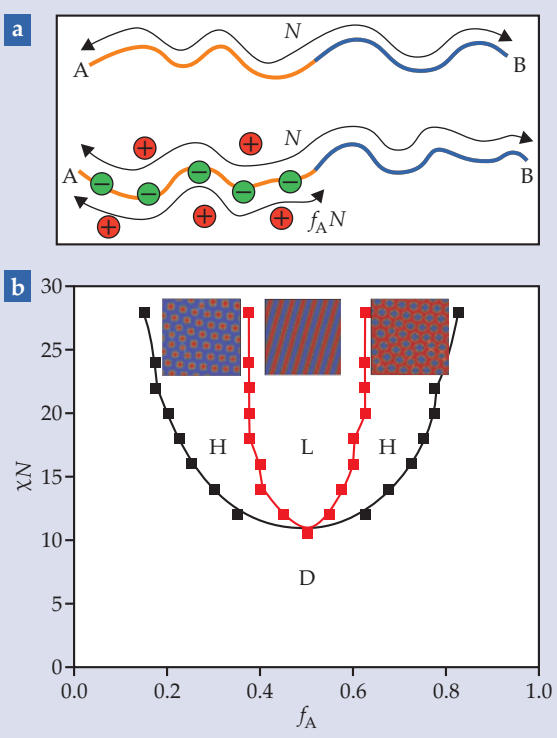

Figure 1. Neutral and charged diblock copolymers **(a)** are characterized by their overall length N and the fraction f_A of that length that's made up of monomer A. **(b)** In the canonical phase diagram for neutral diblock copolymers, if the immiscibility χ of the A and B monomers is sufficiently low, the polymers form a disordered phase (D). At higher immiscibilities, the polymers form self-assembled ordered nanostructures such as hexagonally arranged rods (H) or alternating lamellae (L). (Adapted from ref. 2.)

Monica Olvera de la Cruz and colleagues at Northwestern University have developed a new theory that accurately describes the ion-rich A phase by accounting for correlations among the charged monomers and ions.[2] Tuning the strength of those correlations, which depends, most importantly, on the dielectric constant of the A phase, can induce qualitative changes in the A phase's morphology.

Ionic effects

The canonical phase diagram for neutral diblock copolymers, shown in figure 1b, illustrates how, as a function of the fraction f_A of A monomers and phase immiscibility χ, the polymers can be disordered or can form layered or hexagonal structures. The phase boundaries are derived from self-consistent field theory (SCFT), which is founded on the assumption that as the polymers move around, each one responds to the mean density of all the others—so instead of solving the many-body problem of all the polymers simultaneously, one need only look at the problem of a single polymer moving in an applied field. For neutral-polymer systems, that assumption seems to be good: SCFT has been successfully used for decades to describe various aspects of phase segregation in neutral polymers and copolymers.

Applying SCFT to a charged polymer system means assuming that each charge—whether free or bound to a polymer—feels the average electric field of all the other charges. Such a treatment results in a phase diagram of the same shape as the one in figure 1b, but shifted down by an amount proportional to the fraction of charged monomers in the A phase.[3] That is, the immiscibility χ is replaced by an effective